Research Article

A Wideband Circularly Polarized Antenna with Characteristic Mode Analysis

Lei Chang ⓘ,[1] Ling-Lu Chen ⓘ,[1] Jian-Qiang Zhang,[1] and Dan Li[2]

[1]*No. 36 Research Institute of CETC, Jiaxing 314033, China*
[2]*Academician Workstation of Zhejiang Longyou Gongren Electronics Co., Ltd., Quzhou, Longyou 324014, China*

Correspondence should be addressed to Lei Chang; yutian_1986@163.com

A wideband circularly polarized (CP) antenna is presented to achieve enhanced impedance, axial ratio (AR), and gain bandwidths. The antenna consists of two circular patches, a split-ring microstrip line with six probes, and a circular ground plane. By using these six probes which are placed in sequence on the split-ring microstrip line, the operating bandwidth of the proposed antenna is increased. The characteristic mode method is used to analyze different modes of the antenna and reveal the mechanism of extending the 3-dB AR bandwidth. Measured results show that the proposed antenna obtains an impedance bandwidth of 1.486–2.236 GHz (40.3%) for $S_{11} \leq -18$ dB, a 3-dB AR bandwidth of 1.6–2.2 GHz (31.6%), and a boresight gain of 8.89 ± 0.87 dBic.

1. Introduction

With the development of many wireless systems, such as radar, satellite communication, remote control, and telemetry systems, there are more and more applications of circularly polarized (CP) antennas because CP antennas allow for reduction of multipath fading, avoiding polarization mismatching, and better weather adaptability. A CP annular-ring microstrip antenna using an equal-split power divider is proposed in [1], which has a 3-dB axial ratio (AR) bandwidth of 6%. A CP antenna fed by an L-probe is presented with a 3-dB AR bandwidth of 9%, which uses two stacked folded patches [2]. A square ring slot including four branch slots is applied to produce circular polarization, and a 3-dB AR bandwidth of 8.7% is achieved [3].

However, there is a growing demand for antennas with a wideband AR bandwidth. Therefore, it is necessary to investigate methods of extending AR bandwidth. In [4], an air gap is used to a stacked patch with a single probe feed to enhance the AR bandwidth (20.2%). A coplanar parasitic ring slot patch is introduced to achieve good circular polarization performance with a 3-dB AR bandwidth of 16% [5]. By using an H-shaped patch and a

probe in conjunction with a printed monopole, a 3-dB AR bandwidth of 19.4% is obtained [6]. Based on the meandering feed structures, patch antennas are studied to achieve wide 3-dB AR bandwidths [7–9]. 3-dB AR bandwidths of 13.5% [7], 22.4% [8], and 16.8% [9] are achieved by using a horizontally meandered strip, a 3D meandering strip, and a printed meandering probe, respectively. In [10], a driven patch with a square ring, a 270° loop of microstrip line, and an L-shaped parasitic patch is used to excite four square parasitic patches to achieve a 3-dB AR bandwidth of 28.1%. By using a differentially fed method, a 3-dB AR bandwidth of 31% is obtained [11]. The CP antenna using an n-shaped proximity coupling probe configuration has the impedance and 3-dB AR bandwidths of 25% [12]. In [13], a quasi-magnetic-electric CP patch antenna with a single feed is studied, which can achieve a 3-dB AR bandwidth of 15.3%. An H-shaped microstrip patch and a reactive impedance surface are applied to improve the 3-dB AR bandwidth to 27.5% [14]. Sequential feed methods are also proposed to achieve good circular polarization performance [15–20]. In [15], four cross slots via a microstrip feed line with multiple matching segments are used to excite a square patch, and a 3-dB AR bandwidth of 16% is achieved. Four asymmetric

(a)   (b)

(c)   (d)
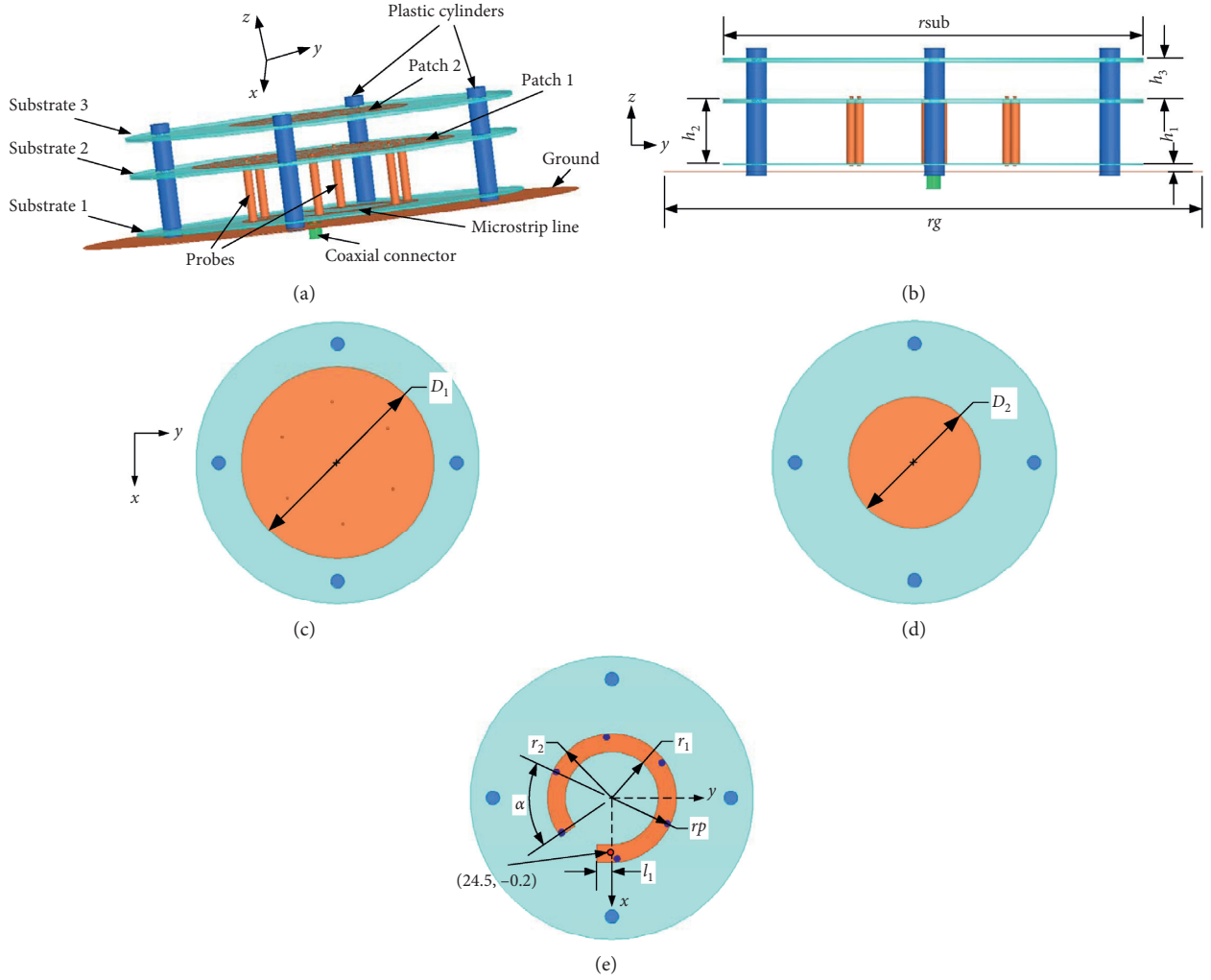
(e)

FIGURE 1: Geometry of the proposed antenna. (a) 3D view, (b) side view, (c) patch 1, (d) patch 2, and (e) microstrip line.

TABLE 1: Dimensions of the proposed antenna.

Parameters	Value
$D1$	85 mm
$r1$	20.5 mm
rp	27 mm
$h1$	2.4 mm
$h3$	12 mm
rg	160 mm
$D2$	58 mm
$r2$	28.5 mm
$l1$	8.5 mm
$h2$	19 mm
α	60°
$rsub$	145 mm

cross slots and a microstrip ring with eight matching segments are applied to obtain an enhanced 3-dB AR bandwidth of 26% [16]. Two coin-shaped patches and a sequential feed structure using four probes are presented in [17], and a 3-dB AR bandwidth of 15.9% is achieved. The 3-dB AR bandwidth is enhanced by using a ring-shaped strip inlaid along the edge of the parasitic patch and two square holes in the center of the main patch and the parasitic one. In [18], a sequential feed structure using four probes which are connected to a microstrip feed line is applied to achieve a wide 3-dB AR bandwidth (16.4%). Two probes connected to a horizontal L-shaped strip are as a sequential feed structure, and a shorting pin is loaded to enhance the 3-dB AR bandwidth (17.9%) [19]. In [20], four slot elements fed by a 4-way sequential-phase feeding network is proposed to achieve a 3-dB AR bandwidth of 15.6%.

In this paper, a wideband right-hand circular polarization (RHCP) antenna with two circular patches and a sequential feed structure is presented. By increasing the number of probes of the sequential feed structure from 4 to 6, the impedance and 3-dB AR bandwidths are improved. The effects of the number of probes on the antenna performance are analyzed by the characteristic mode (CM) method. The proposed antenna exhibits a 3-dB AR bandwidth of 1.6–2.2 GHz (31.6%) and a good impedance matching performance in the band of 1.486–2.236 GHz (40.3%) for $S_{11} \leq -18$ dB.
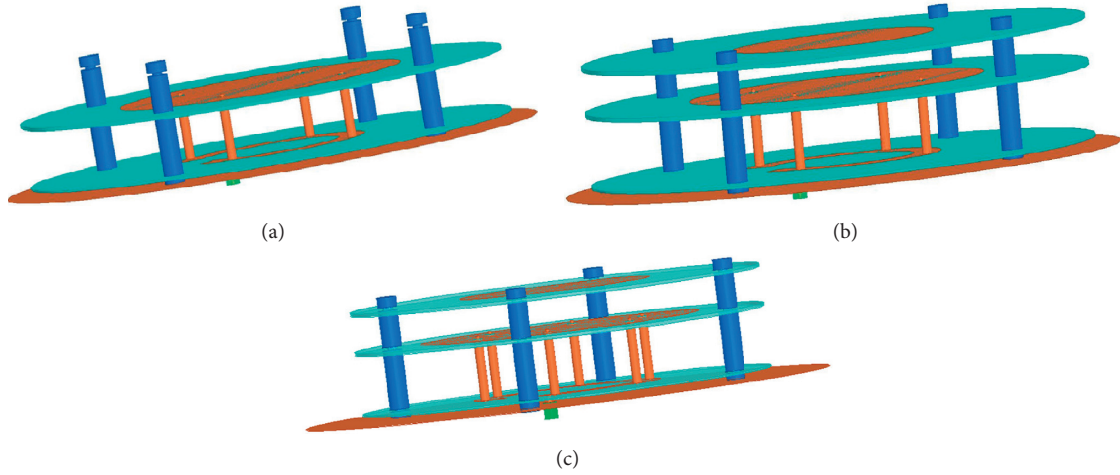
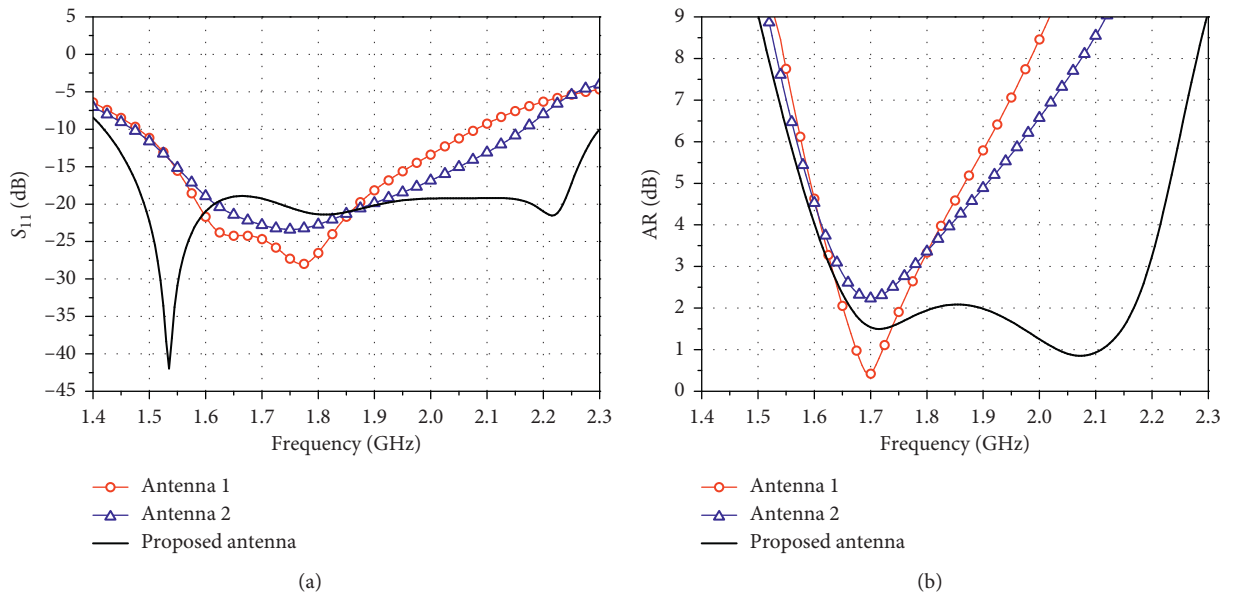FIGURE 2: Three CP antennas. (a) Antenna 1. (b) Antenna 2. (c) Proposed antenna.

FIGURE 3: Simulated results of the three CP antennas. (a) S_{11} and (b) AR.

2. Antenna Design

The geometry of the proposed antenna is depicted in Figure 1, and the simulated results are obtained by using HFSS. The diameters of patch 1 and patch 2 are D_1 and D_2, respectively. The distance between the two patches is h_3. The inner and outer radii of the split-ring microstrip line are r_1 and r_2, respectively. The beginning of the split-ring microstrip line contains a rectangular section with length l_1. The rectangular section is introduced to enhance the impedance bandwidth. The distance between patch 1 and the split-ring microstrip line is h_2. The split-ring microstrip line, patch 1, and patch 2 are printed on the substrate F₄BMX220 with $\varepsilon_r = 2.2$ and $\tan\delta = 0.0007$. Substrate 1, substrate 2, and substrate 3 have a thickness of 0.5 mm, 1 mm, and 1 mm, respectively. The diameter of the three substrates is *rsub*. Six probes with a diameter of 2.8 mm are used to feed patch 1,

which are placed in sequence on the split-ring microstrip line. The probes are distributed along an arc line with radius *rp*. The angle between the two adjacent probes is α. The number of probes and the angle α affect the CP performance and impedance bandwidth greatly. The diameter of the ground is *rg*. The distance between the ground and the split-ring microstrip line is h_1. The detailed dimensions of the proposed antenna are shown in Table 1.

Three prototypes of the CP antennas are created to exhibit the design process of the proposed antenna, as shown in Figure 2. Antenna 1 has four probes and no parasitic patch. Antenna 2 includes a circular parasitic patch. The proposed antenna contains six probes and a circular parasitic patch. The simulated S_{11} and boresight AR of the three CP antennas are shown in Figure 3.

For antenna 1, by using the sequential feed structure with four probes, the RHCP wave is obtained. Antenna 1 achieves
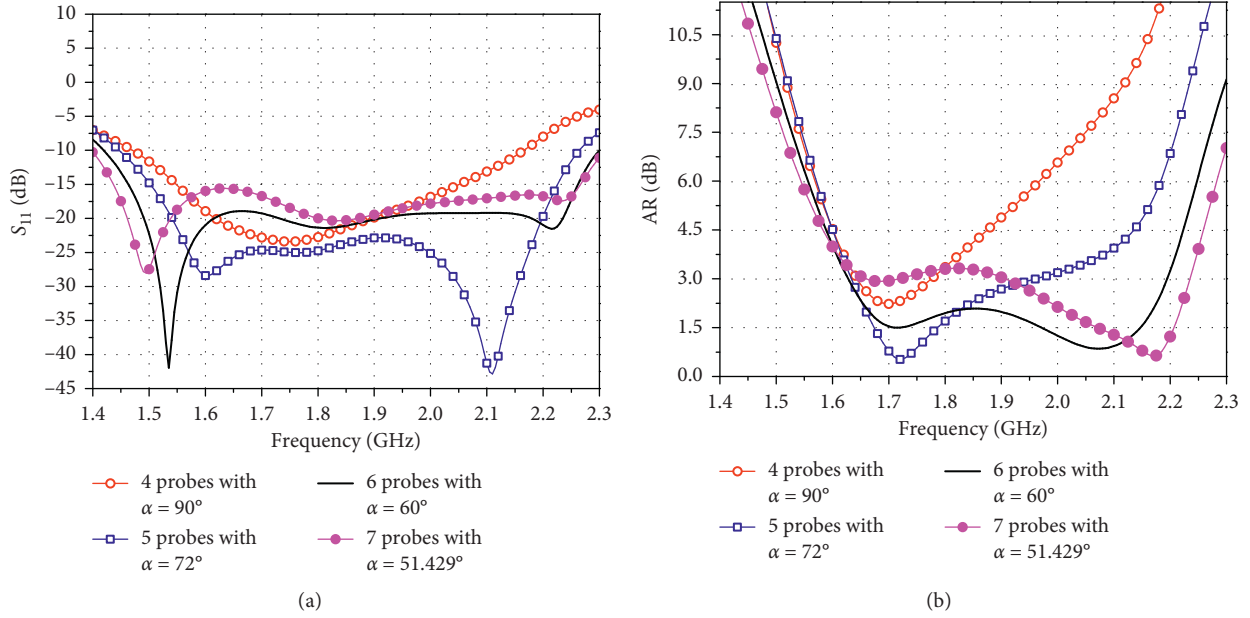
(a)

(b)

Figure 4: Effects of the number of probes on (a) S_{11} and (b) AR.
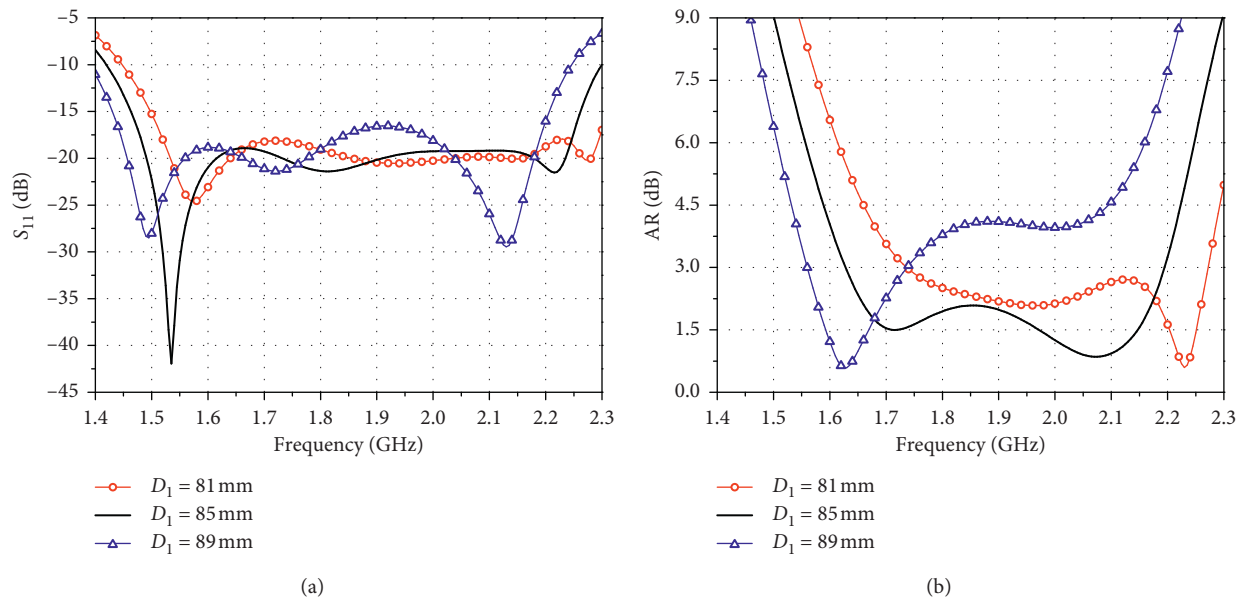

(a)

(b)

Figure 5: Effects of the diameter D_1 of patch 1 on (a) S_{11} and (b) AR.

an impedance bandwidth of 19.28% for $S_{11} \leq -18$ dB and 3-dB AR bandwidth of 9.36%. The impedance and 3-dB AR bandwidths are still narrow.

By adding a parasitic patch, the impedance bandwidth of antenna 2 is increased to 21.41% for $S_{11} \leq -18$ dB. The 3-dB AR bandwidth is only 8.19%. However, the AR of antenna 2 in the band of 1.8–2.3 GHz is better than that of antenna 1.

For the proposed antenna, the number of the probes is increased from 4 to 6, and the impedance and 3-dB AR bandwidths are improved to 41% (1.483–2.247 GHz) for

$S_{11} \leq -18$ dB and 29.6% (1.628–2.193 GHz). It can be observed that the number of probes has a significant effect on the impedance and 3-dB AR bandwidths.

2.1. Effects of the Number of Probes. We study the performance of the antenna when the number of probes is 4, 5, 6, and 7 with $\alpha = 90°$, $72°$, $60°$, and $51.429°$, respectively, as shown in Figure 4. For traditional four probes with $\alpha = 90°$, the 3-dB AR bandwidth is only 7.8% and the impedance bandwidth for $S_{11} \leq -18$ dB is 21.2%. To extend the 3-dB
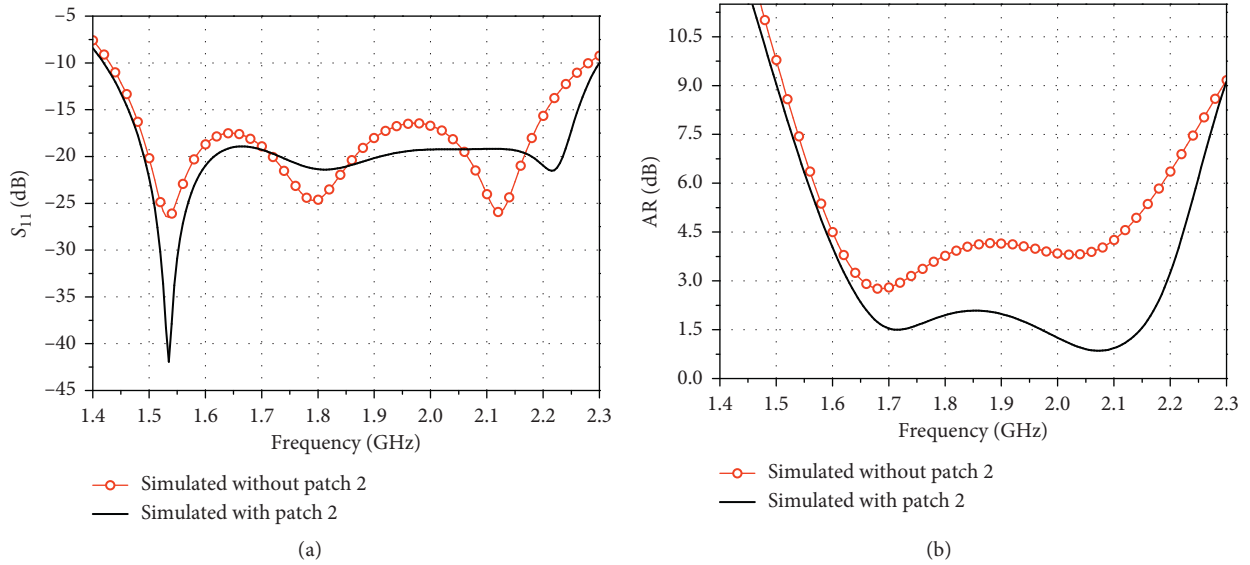
(a)

(b)

FIGURE 6: Effects of patch 2 on (a) S_{11} and (b) AR.
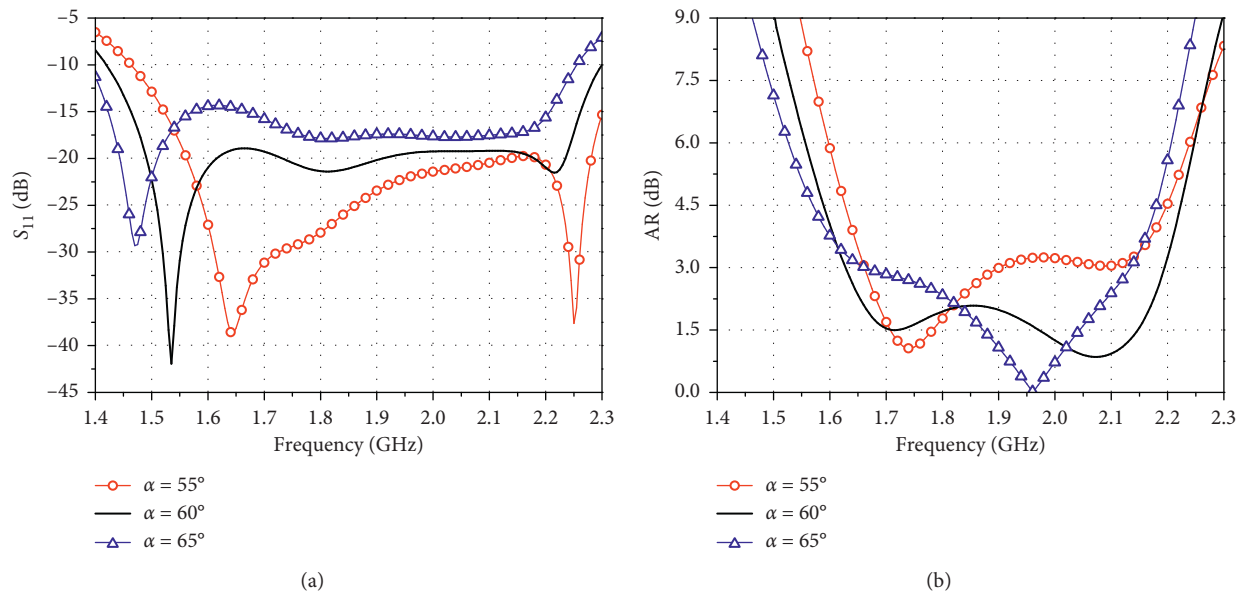

(a)

(b)

FIGURE 7: Effects of the angle α on (a) S_{11} and (b) AR.

AR bandwidth, we proposed a new method to achieve an enhanced AR bandwidth by increasing the number of probes.

When five probes with $\alpha = 72°$ are used, the impedance bandwidth for $S_{11} \leq -21$ dB is 34.6% (1.547–2.194 GHz). However, the 3-dB AR bandwidth is only 18.3%. The impedance bandwidth of 41% for $S_{11} \leq -18$ dB and the 3-dB AR bandwidth of 29.6% are achieved when six probes with $\alpha = 60°$ are introduced. As the number of probes

increases to seven ($\alpha = 51.429°$), the impedance matching becomes worse and the 3-dB AR bandwidth is only 15.9%.

2.2. Effects of Patch 1 and Patch 2. Patch 1 is a main radiation patch, and patch 2 is a parasitic patch. The simulated results of S_{11} and AR by varying D_1 are shown in Figure 5. As D_1 increases, the operating frequency band of the antenna is shifted to a lower frequency.
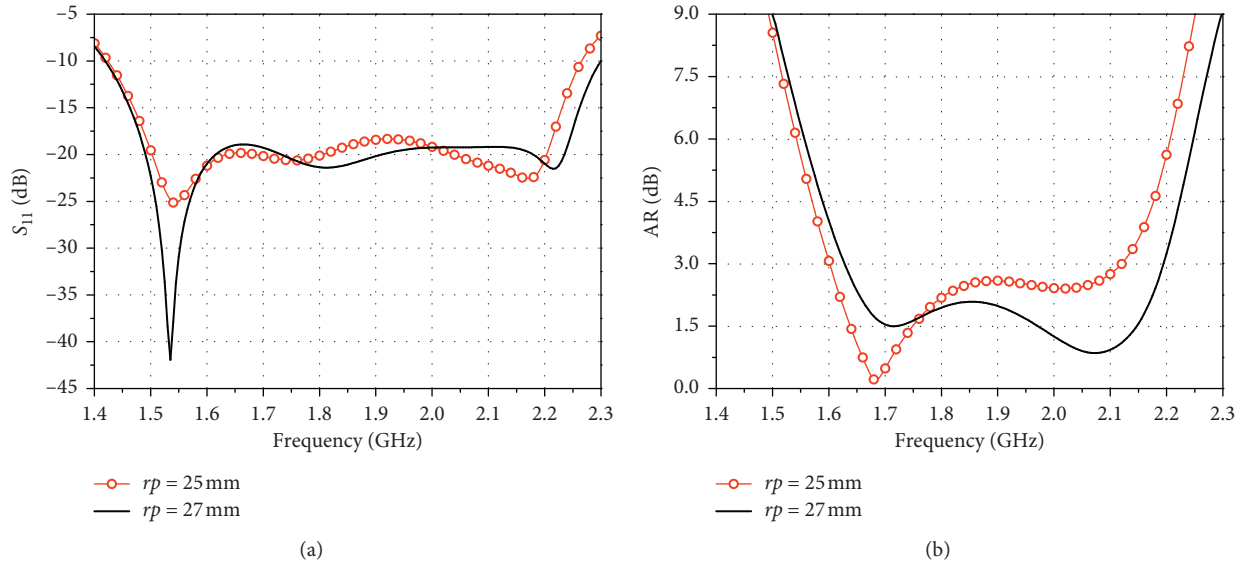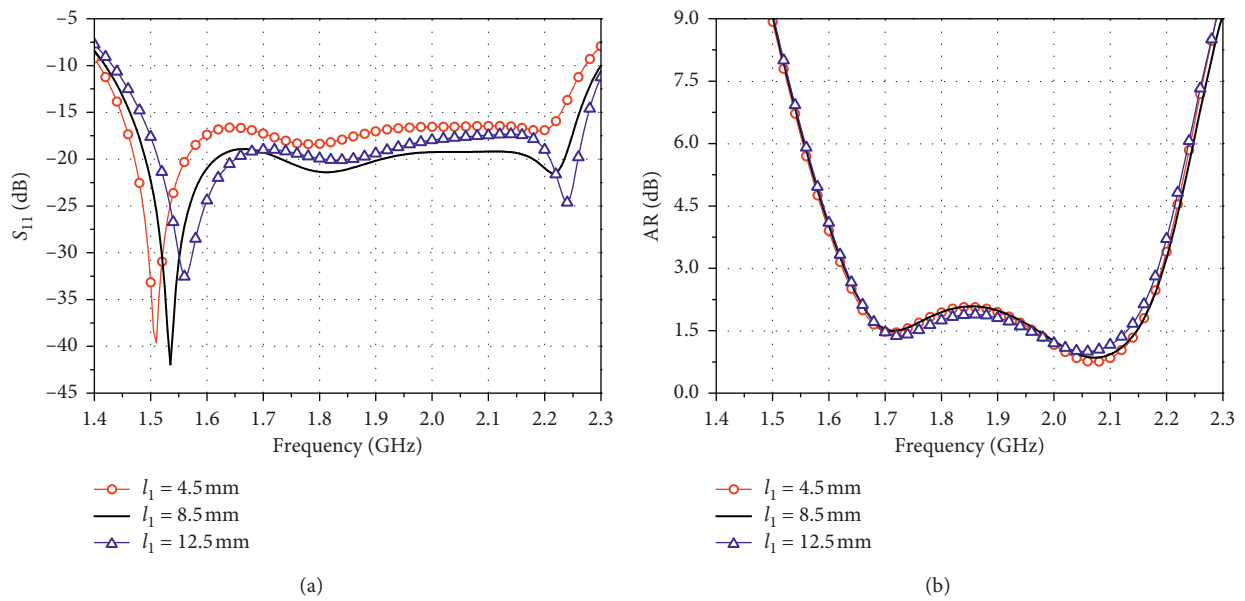
(a)

(b)

FIGURE 8: Effects of the radius rp on (a) S_{11} and (b) AR.

(a)

(b)

FIGURE 9: Effects of the length l_1 on (a) S_{11} and (b) AR.

Figure 6 shows the effects of patch 2 on the performance of S_{11} and boresight AR. It is shown that patch 2 has a significant effect on the AR, especially in the high-frequency band.

2.3. Effects of the Sequential Feed Structure.

The parameters of the angle α, the length l_1, and the radius rp are investigated to further illustrate the antenna design process.

The effects of the angle α on the performance of S_{11} and boresight AR are shown in Figure 7. It is shown that the maximum value of S_{11} in the band of 1.55–2.25 GHz is increased and the low cutoff frequency is shifted to a lower frequency as the angle α increases. Decreasing α makes the

AR become worse in the high-frequency band. Thus, $\alpha = 60°$ was chosen.

As shown in Figure 8(a), the radius rp has a slight effect on the impedance matching. However, the AR in the band of 1.8–2.2 GHz becomes worse as rp decreases, as shown in Figure 8(b).

The effects of the length l_1 of the rectangular section on the split-ring microstrip line are shown in Figure 9. The length l_1 has a slight effect on the AR. Compared with $l_1 = 8.5$ mm, the impedance bandwidth is shifted down and the impedance matching in the band of 1.6–2.2 GHz becomes worse with $l_1 = 4.5$ mm; while with $l_1 = 12.5$ mm, the impedance matching in the band of 1.7–2.2 GHz becomes worse.
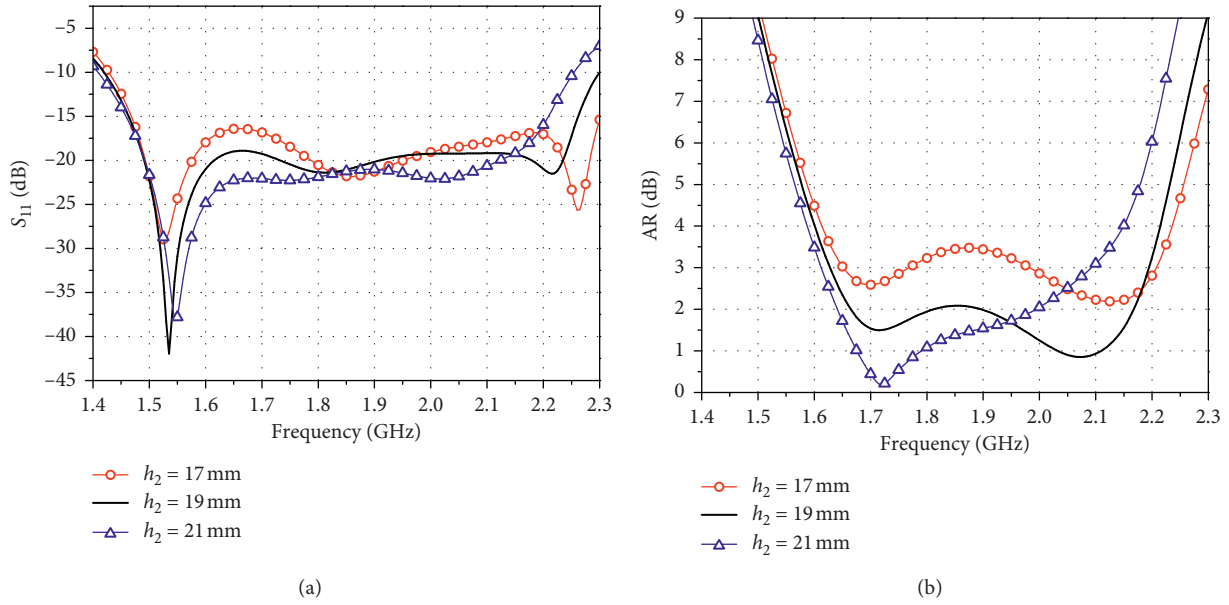
(a)

(b)

FIGURE 10: Effects of the height h_2 on (a) S_{11} and (b) AR.
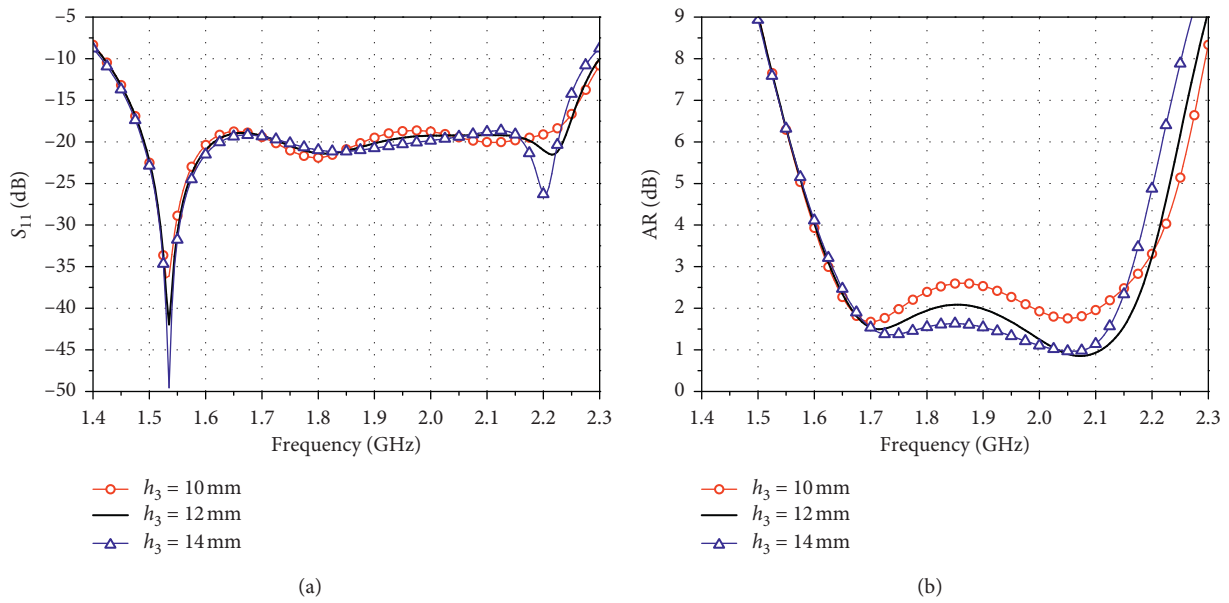

(a)

(b)

FIGURE 11: Effects of the height h_3 on (a) S_{11} and (b) AR.

2.4. Effects of the Height h_2 and h_3. The effects of varying height of patch 1 and patch 2 on the performance of S_{11} and boresight AR are shown in Figures 10 and 11, respectively.

As the height h_2 decreases, the impedance matching and boresight AR in the operating band get worse. Increasing h_2 makes the impedance matching and boresight AR better, but narrows the operating bandwidth.

A slight effect of the height h_3 on the impedance matching has been observed. However, the height h_3 has a significant effect on the boresight AR. Increasing h_3 greatly degrades the 3-dB AR bandwidth. When h_3 is reduced to 10 mm, the boresight AR deteriorates in the operating band.

Figure 12 shows the surface current distribution on patch 1 and patch 2 at 1.91 GHz. It is obvious that the vector current rotates counterclockwise in a circular path, which depicts RHCP.

2.5. Characteristic Mode Analysis (CMA). In order to illustrate the operating principle of the antenna, CMA is carried out using FEKO.

When four probes with $\alpha = 90°$ are used, the mode current distribution at 1.72 and 1.96 GHz is shown in Figure 13. Figure 13(a) shows that mode 1 is orthogonal to modes 3 and 4 at 1.72 GHz. Thus, the CP radiation
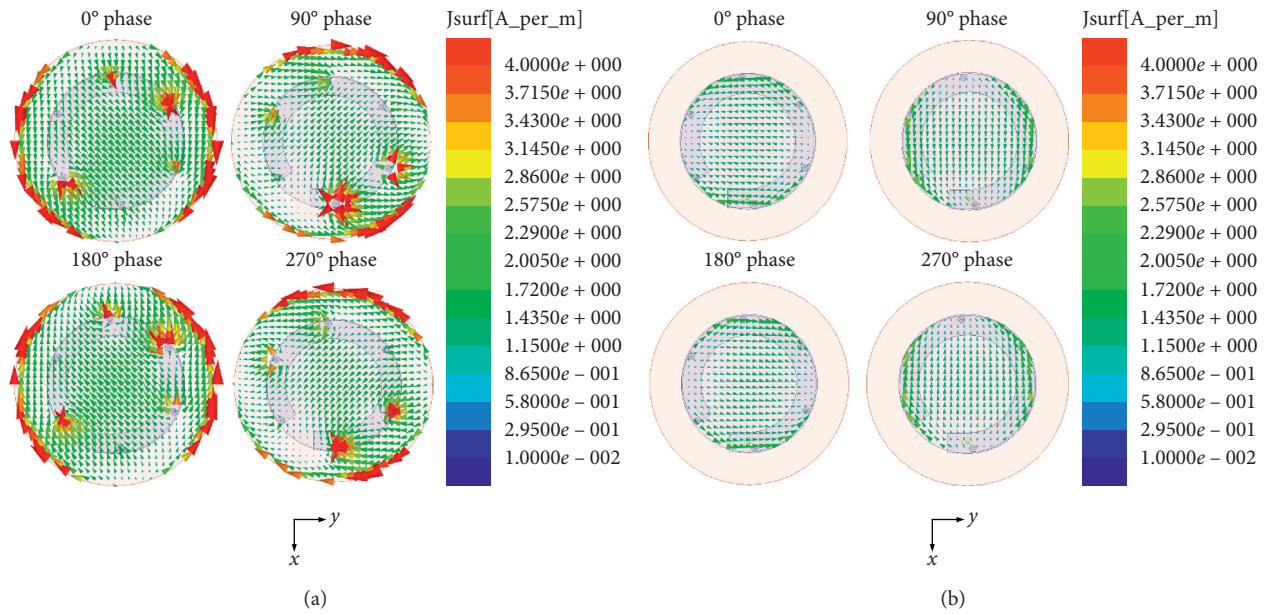
FIGURE 12: The surface current distribution on (a) patch 1 and (b) patch 2 at 1.91 GHz.
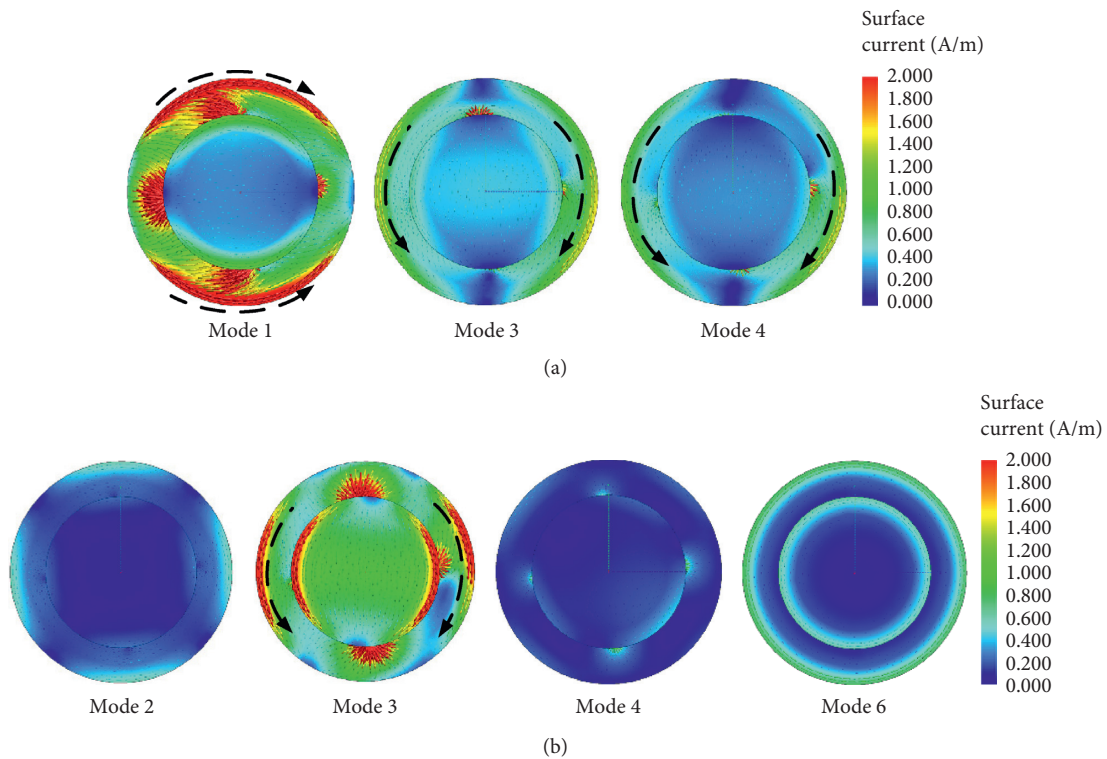

FIGURE 13: Modal current distribution of the antenna with four probes at (a) 1.72 GHz and (b) 1.96 GHz.

characteristics are obtained by modes 1, 3, and 4. However, modes 1 and 5 cannot be excited, and there is no mode that is orthogonal to mode 3 at 1.96 GHz, as shown in Figure 13(b). This leads to the deterioration of AR in the high-frequency band.

Figure 14 shows the modal current distribution of the proposed antenna with six probes at 1.72 and 1.96 GHz. We

can see that mode 2 is orthogonal to modes 3 and 5 at 1.72 GHz, as well as mode 3 is orthogonal to mode 5 at 1.96 GHz. Thus, when the six probes are used, the antenna can obtain a wide AR bandwidth. Furthermore, mode 5 has intense current at patch 2 at 1.96 GHz. This indicates that patch 2 has a great influence on the CP radiation in the high-frequency band.
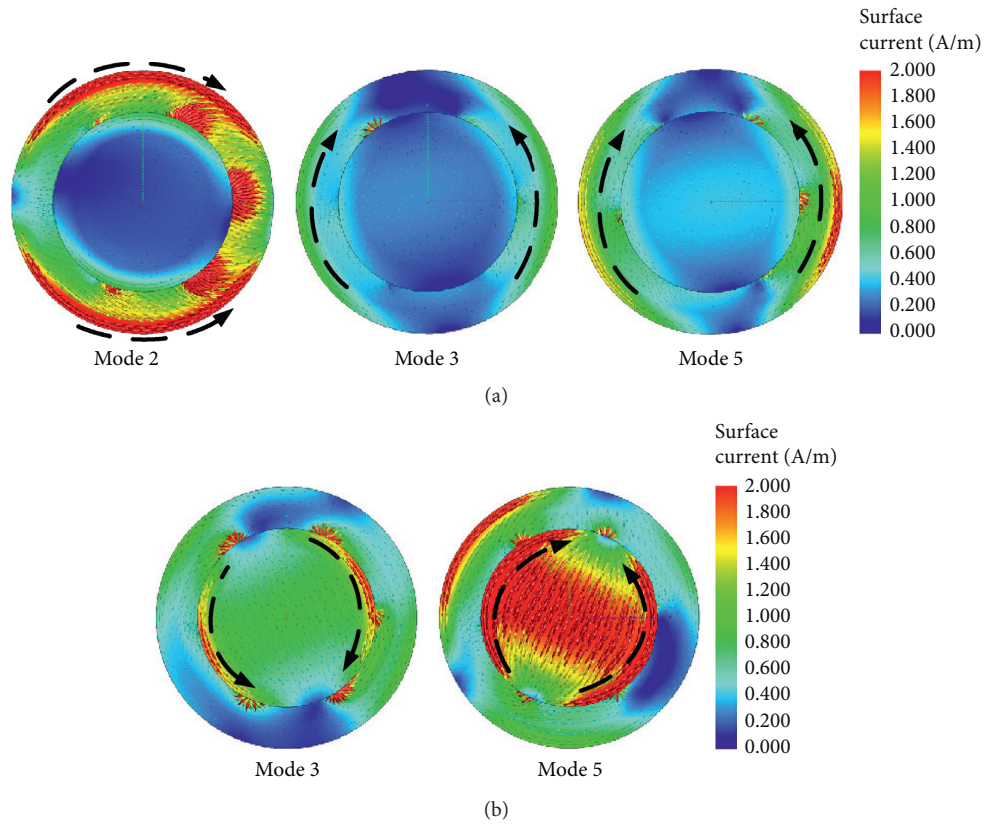
Mode 2   Mode 3   Mode 5

(a)

Mode 3   Mode 5

(b)

Figure 14: Modal current distribution of the antenna with six probes at (a) 1.72 GHz and (b) 1.96 GHz.

Mode 2   Mode 3   Mode 5
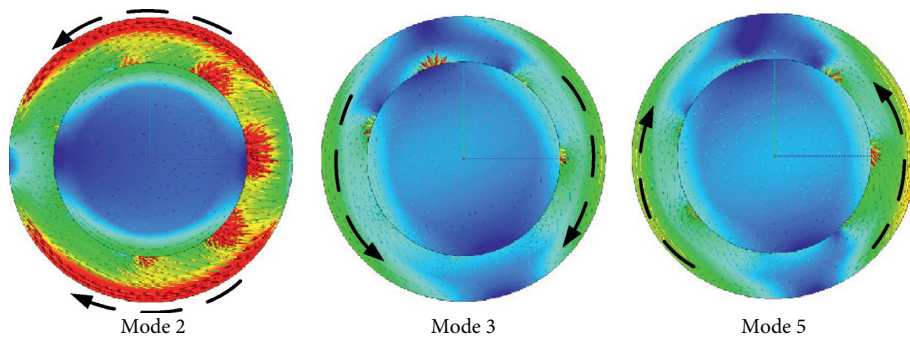
Figure 15: Modal current distribution of the antenna with seven probes at 1.72 GHz.

When seven probes with $\alpha = 51.429°$ are used, the AR in the low-frequency band has deteriorated. The mode current distribution at 1.72 GHz is shown in Figure 15. It is shown that mode 2 is orthogonal to modes 3 and 5. However, the current in modes 3 and 5 flows in opposite directions, which leads to the amplitude imbalance between the orthogonal modes, resulting in the deterioration of the AR.

3. Measured Results and Discussion

Figure 16 shows the fabricated prototype. S_{11} was measured by using the Rohde & Schwarz ZVT 8 vector network analyzer. Radiation patterns, gain, and AR were measured in an anechoic chamber.

The simulated and measured S_{11} of the proposed antenna are shown in Figure 17(a). The measured impedance bandwidth for $S_{11} \leq -18$ dB is 40.3% from 1.486 to 2.236 GHz. Figure 17(b) shows the simulated and measured boresight AR. The measured bandwidth for AR ≤ 3 dB is 31.6%, covering 1.6 to 2.2 GHz. Figure 17(c) shows the measured boresight gain compared with the simulated result. The proposed antenna shows a stable measured gain of 8.89 ± 0.87 dBic within the 3-dB AR bandwidth.

The simulated and measured radiation patterns of two principal planes at 1.65, 1.9, and 2.15 GHz are shown in
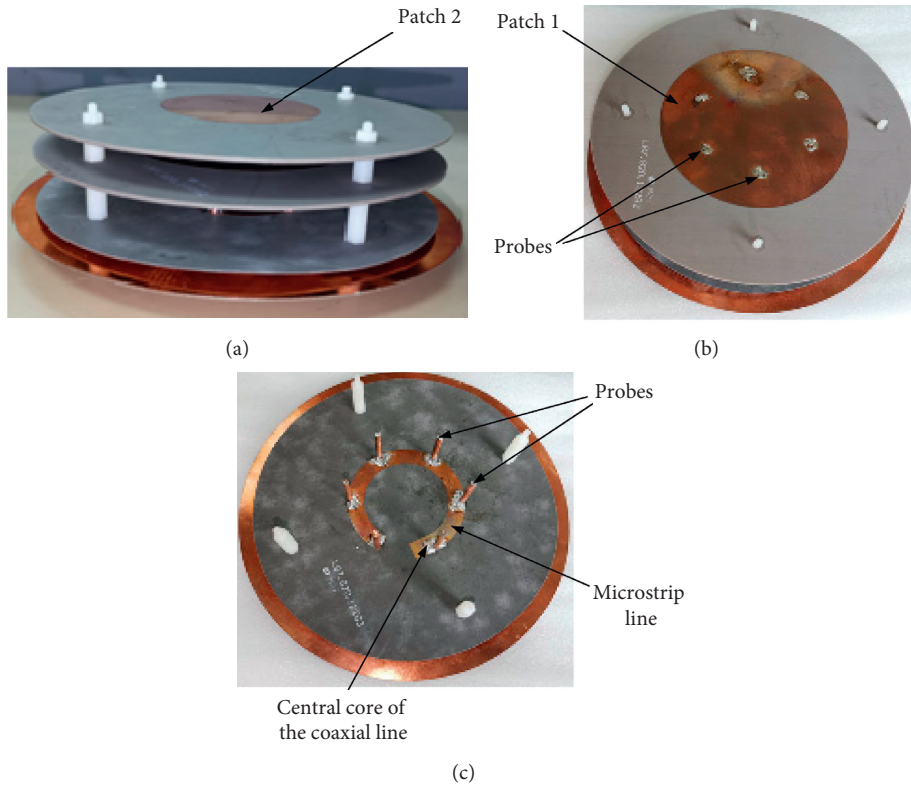
(a)

(b)

(c)

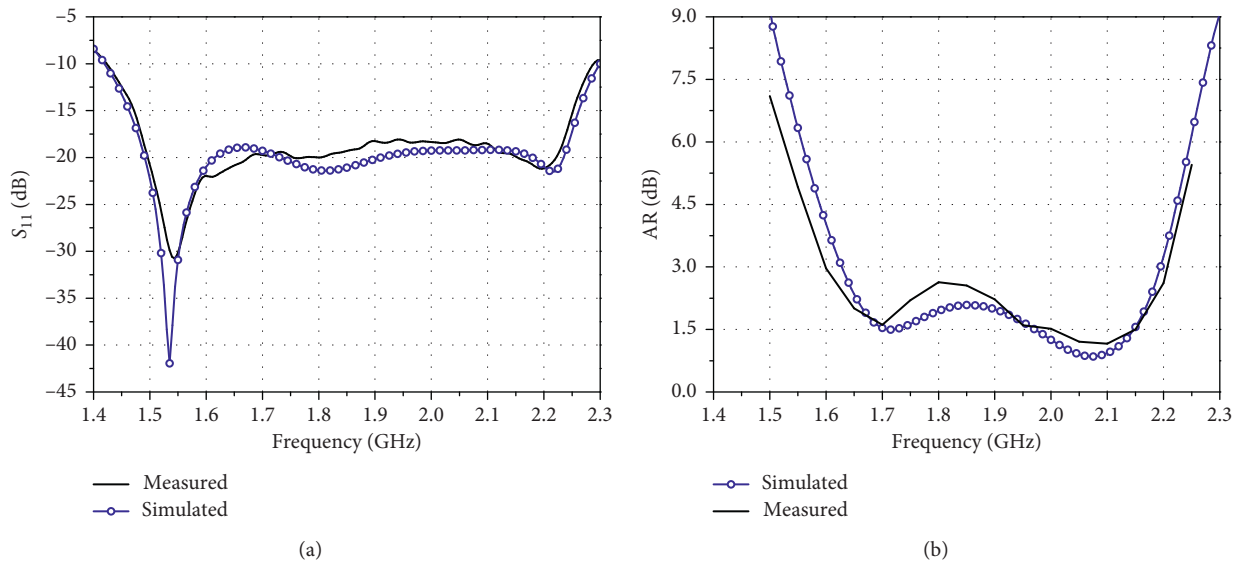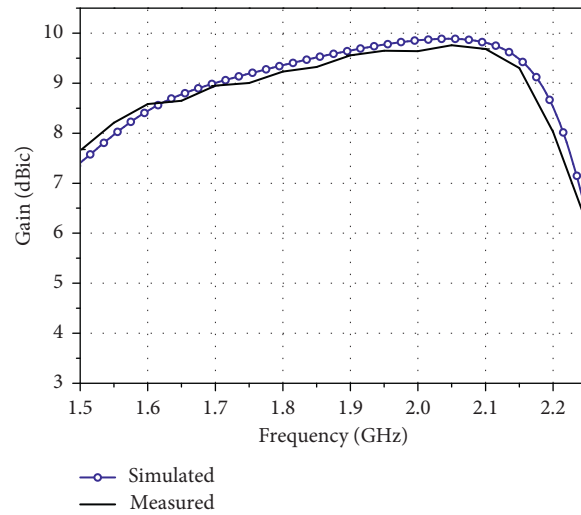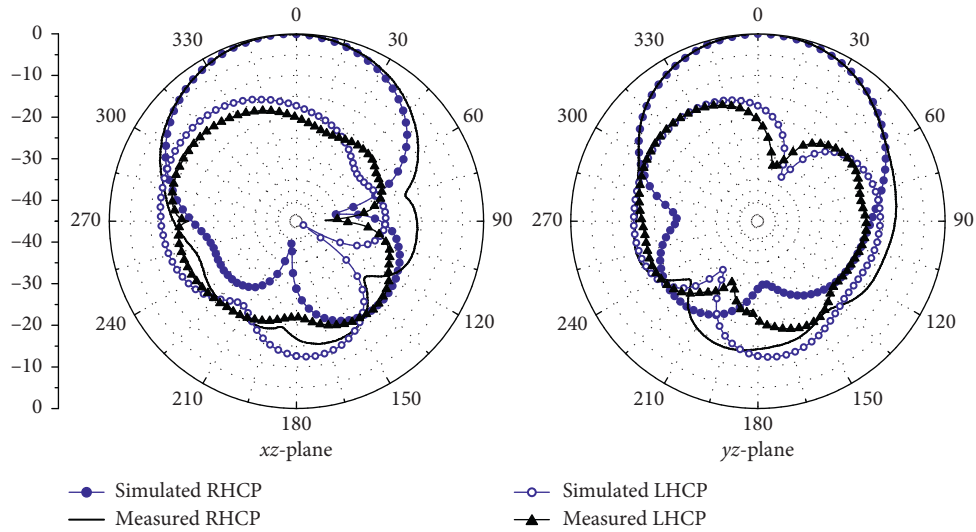FIGURE 16: Photograph of the fabricated antenna.
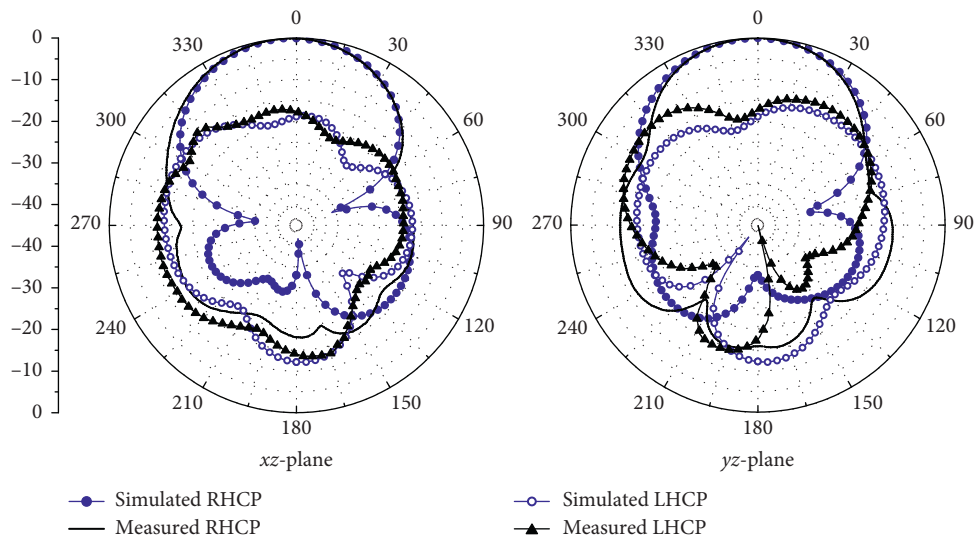

(a)

(b)

FIGURE 17: Continued.

(c)

FIGURE 17: Measured and simulated results: (a) S_{11}, (b) AR, and (c) gain.
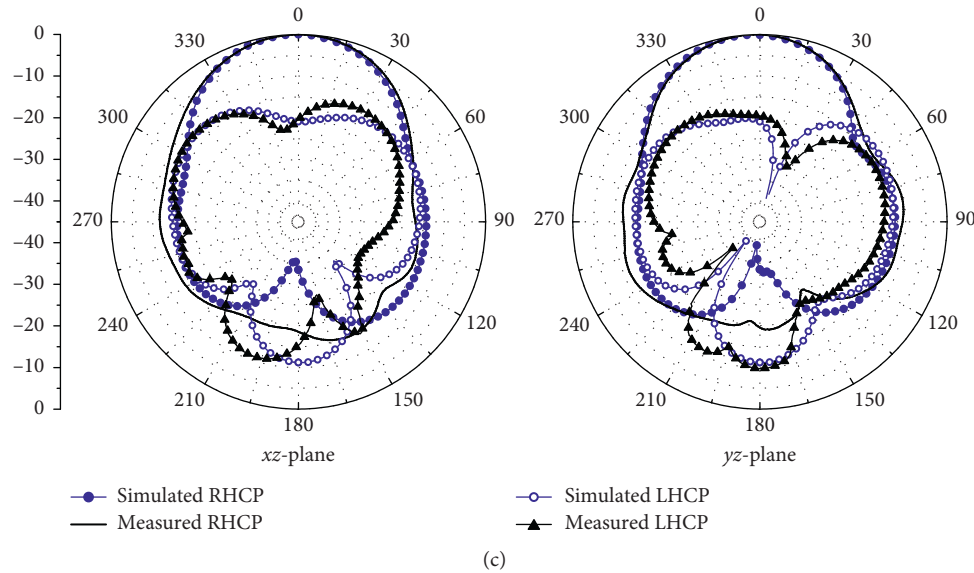

(a)

(b)

FIGURE 18: Continued.

FIGURE 18: Measured and simulated radiation patterns of the proposed antenna at (a) 1.65, (b) 1.9, and (c) 2.15 GHz.

TABLE 2: Comparisons of the proposed and other CP antennas.

Ref. year	Dimension of patch × height of antenna (λ_{ARd})	Impedance matching	Impedance bandwidth	3-dB AR bandwidth	Gain (dBic)
[5] 2014	$\phi 0.55 \times 0.14$	$S_{11} \leq -14$ dB	27% (1.45–1.9 GHz)	16% (1.51–1.77 GHz)	About 7.7–8
[9] 2014	$0.24 \times 0.24 \times 0.13$	$S_{11} \leq -10$ dB	42.3% (4.1–6.3 GHz)	16.8% (5.05–5.98 GHz)	Peak gain: 6.7
[10] 2017	About $0.27 \times 0.27 \times 0.07$	$S_{11} \leq -10$ dB	38% (5–7.35 GHz)	28.1% (5.32–7.06 GHz)	Peak gain: 8.4
[11] 2018	$0.32 \times 0.32 \times 0.21$	$S_{11} \leq -10$ dB	60.5% (1.5–2.8 GHz)	31% (1.74–2.38 GHz)	6.5 ± 0.4
*[12] 2017	$0.45 \times 0.44 \times 0.11$	$S_{11} \leq -10$ dB	25% (2.15–2.75 GHz)	25% (2.1–2.7 GHz)	Peak gain: 8.3
[13] 2019	$0.67 \times 0.45 \times 0.21$	$S_{11} \leq -10$ dB	31.7% (2.35–3.3 GHz)	15.3% (2.6–3.06 GHz)	6.46–7.64
**[14] 2018	$0.15 \times 0.15 \times 0.09$	$S_{11} \leq -10$ dB	44.5% (4.64–7.3 GHz)	27.5% (4.55–6 GHz)	Peak gain: 7.2
[15] 2014	$0.31 \times 0.31 \times 0.19$	$S_{11} \leq -10$ dB	24% (3.2–4.1 GHz)	16% (3.5–4 GHz)	Peak gain: 9.6
[16] 2015	$\phi 0.34 \times 0.16$	$S_{11} \leq -10$ dB	29.7% (3–4.1 GHz)	21.6% (3.3–4.1 GHz)	Peak gain: 8.6
[19] 2014	$0.35 \times 0.35 \times 0.08$	$S_{11} \leq -10$ dB	23.6% (2.09–2.65 GHz)	17.9% (2.18–2.61 GHz)	About 8.5
[20] 2018	$1.7 \times 1.7 \times 0.22$	$S_{11} \leq -10$ dB	53.1% (3.9–6.72 GHz)	15.6% (4.73–5.53 GHz)	12.4–13.4
Prop.	$\phi 0.45 \times 0.18$	$S_{11} \leq -18$ dB	40.3% (1.486–2.236 GHz)	31.6% (1.6–2.2 GHz)	8.02–9.76

λ_{ARd} is the free-space wavelength at the starting frequency of the 3-dB AR bandwidth. *λ_{ARd} is the free-space wavelength at 2.15 GHz. **λ_{ARd} is the free-space wavelength at 4.64 GHz.

Figure 18. The 3-dB beamwidth is more than 45° for both planes.

Table 2 summarizes some key indicators of the proposed antenna and other wideband CP antennas. The antenna proposed in [14] is fed by a single feed point. The antenna proposed in [10] is fed equivalently by two feed points. To improve the AR of the antenna in [14], a reactive impedance surface is used. To improve the AR of the antenna in [10], an L-shaped parasitic patch and four parasitic patches are used. In [11], a wide 3-dB AR bandwidth of 31% is achieved by generating an equivalent four-point feeding. It is observed that the more the feeding points, the easier it is to obtain a wider 3-dB AR bandwidth (27.5% in [14], 28.1% in [10], and 31% in [11]) and a wider impedance bandwidth (44.5%% in [14], 38% in [10], and 60.5% in [11]). In this paper, an

equivalent six-point feeding and a parasitic patch are used to extend the impedance and 3-dB AR bandwidths. Compared with the CP antennas in [5, 9–16, 19, 20], the proposed antenna has a wider 3-dB AR bandwidth and better impedance matching. The peak gain of the proposed antenna is 9.76 dBic, which is a good result. Although the antenna in [20] has a greater peak gain, the size is larger than that of the proposed antenna. The size of the proposed antenna is also competitive.

4. Conclusion

In this paper, a wideband CP antenna is studied and its advantages in impedance matching and CP radiation performance are discussed in detail. By introducing six probes, a

parasitic patch, and a split-ring microstrip line containing a rectangular section, the impedance bandwidth of 40.3% for $S_{11} \leq -18$ dB and the 3-dB AR bandwidth of 31.6% are achieved, which shows a great improvement in the operating bandwidth. A peak gain of 9.76 dBic and unidirectional radiation patterns are also achieved.

Data Availability

The data used to support the findings of this study are included within the article.

Conflicts of Interest

The authors declare that they have no conflicts of interest.

Acknowledgments

References

[1] X. Chen, G. Fu, S.-X. Gong, Y.-L. Yan, and W. Zhao, "Circularly polarized stacked annular-ring microstrip antenna with integrated feeding network for UHF RFID readers," *IEEE Antennas and Wireless Propagation Letters*, vol. 9, pp. 542–545, 2010.

[2] X. H. Tang, K. L. Lau, Q. Xue, and Y. L. Long, "Miniature circularly polarised patch antenna," *Electronics Letters*, vol. 46, no. 6, pp. 391-392, 2010.

[3] T.-N. Chang, J.-M. Lin, and Y. G. Chen, "A circularly polarized ring-antenna fed by a serially coupled square slot-ring," *IEEE Transactions on Antennas and Propagation*, vol. 60, no. 2, pp. 1132–1135, 2012.

[4] S. M. Kim and W. G. Yang, "Single feed wideband circular polarised patch antenna," *Electronics Letters*, vol. 43, no. 13, pp. 703-704, 2007.

[5] S. Fu, Q. Kong, S. Fang, and Z. Wang, "Broadband circularly polarized microstrip antenna with coplanar parasitic ring slot patch for L-band satellite system application," *IEEE Antennas and Wireless Propagation Letters*, vol. 13, pp. 943–946, 2014.

[6] K. L. Chung, "A wideband circularly polarized H-shaped patch antenna," *IEEE Transactions on Antennas and Propagation*, vol. 58, no. 10, pp. 3379–3383, 2010.

[7] Z. Wang, S. Fang, S. Fu, and S. Jia, "Single-fed broadband circularly polarized stacked patch antenna with horizontally meandered strip for universal UHF RFID applications," *IEEE Transactions on Microwave Theory and Techniques*, vol. 59, no. 4, pp. 1066–1073, 2011.

[8] X. H. Tang, Y. L. Long, H. Wong, and K. L. Lau, "Broadband circularly-polarised patch antenna with 3D meandering strip feed," *Electronics Letters*, vol. 47, no. 19, pp. 1060–1062, 2011.

[9] Q. W. Lin, H. Wong, X. Y. Zhang, and H. W. Lai, "Printed meandering probe-fed circularly polarized patch antenna with wide bandwidth," *IEEE Antennas and Wireless Propagation Letters*, vol. 13, pp. 654–657, 2014.

[10] W.-W. Yang, W.-J. Sun, W. Qin, J.-X. Chen, and J.-Y. Zhou, "Broadband circularly polarised stacked patch antenna with integrated dual-feeding network," *IET Microwaves, Antennas & Propagation*, vol. 11, no. 12, pp. 1791–1795, 2017.

[11] Z. H. Tu, K. G. Jia, and Y. Y. Liu, "A differentially fed wideband circularly polarized antenna," *IEEE Antennas and Wireless Propagation Letters*, vol. 17, no. 4, pp. 861–864, 2018.

[12] Z.-Y. Zhang and K.-L. Wu, "A circularly polarized table-like air patch antenna with four grounded metal legs," *IEEE Antennas and Wireless Propagation Letters*, vol. 16, pp. 190–193, 2017.

[13] Z. Li, J. Liu, and Y. Long, "A quasi-magnetic-electric circularly polarized antenna with wide bandwidth," *IEEE Antennas and Wireless Propagation Letters*, vol. 18, no. 10, pp. 2145–2149, 2019.

[14] J. Chatterjee, A. Mohan, and V. Dixit, "Broadband circularly polarized H-shaped patch antenna using reactive impedance surface," *IEEE Antennas and Wireless Propagation Letters*, vol. 17, no. 4, pp. 625–628, 2018.

[15] C. Zhang, X. Liang, X. Bai, J. Geng, and R. Jin, "A broadband dual circularly polarized patch antenna with wide beamwidth," *IEEE Antennas and Wireless Propagation Letters*, vol. 13, pp. 1457–1460, 2014.

[16] C. Zhang, J. Geng, B. Zhou, X. Liang, and R. Jin, "A broadband single-feed circularly polarized patch antenna with wide beamwidth," *International Journal of Antennas and Propagation*, vol. 2015, Article ID 740274, 10 pages, 2015.

[17] X. Liu, Y. Liu, and M. M. Tentzeris, "A novel circularly polarized antenna with coin-shaped patches and a ring-shaped strip for worldwide UHF RFID applications," *IEEE Antennas and Wireless Propagation Letters*, vol. 14, pp. 707–710, 2015.

[18] Z. N. Chen, X. M. Qing, and H. L. Chung, "A universal UHF RFID reader antenna," *IEEE Transactions on Microwave Theory and Techniques*, vol. 57, no. 5, pp. 1275–1282, 2009.

[19] J. Wu, X. Ren, Z. Wang, and Y. Yin, "Broadband circularly polarized antenna with L-shaped strip feeding and shorting-pin loading," *IEEE Antennas and Wireless Propagation Letters*, vol. 13, pp. 1733–1736, 2014.

[20] C. Zhou and S. W. Cheung, "High-gain windmill-shaped circularly polarized antenna using the high-order mode and ground-edge diffraction," *IEEE Antennas and Wireless Propagation Letters*, vol. 17, no. 3, pp. 368–372, 2018.